Time-domain Dynamic-performance-improvement Method for Pulse-width-modulated DC-DC Converters Based on Eigenvalue and Eigenvector Sensitivity*

*Hong Li**, *Zexi Zhou*, *Jinchang Pan and Qian Liu*

(School of Electrical Engineering, Beijing Jiaotong University, Beijing 100044, China)

Abstract: For pulse-width modulated (PWM) DC-DC converters, the input voltage fluctuation and load variation in practical applications make it necessary for them to have better dynamic performance to meet the regulation requirements of the system. The dynamic-performance-improvement method for PWM DC-DC converters is mainly based on indirect dynamic performance indices, such as the gain margin and phase margin. However, both settling time and overshoot in the time domain are important in practical engineering. This makes it difficult for designers to obtain a clear understanding of the time-domain dynamic performance that can be achieved with improved control. In this study, a direct analysis of the time-domain dynamic characteristic of PWM DC-DC converters is performed. A dynamic-performance-improvement method based on eigenvalues and eigenvector sensitivity (E^2S-based DPIM) is proposed to directly improve the time-domain dynamic performance index of PWM DC-DC converters. By considering a boost converter with proportional-integral control as an example, an additional virtual inductor current feedback control was designed using the proposed dynamic-performance-improvement method. Simulation and experimental results verify the validity and accuracy of the proposed dynamic-performance-improvement method.

Keywords: PWM DC-DC converter, time-domain dynamic-performance-improvement method, eigenvalue and eigenvector sensitivity, additional virtual inductor current feedback control

1 Introduction

DC-DC converters are indispensable in consumer electronics, aircraft electrical power supplements, and other engineering applications. In a digital still camera, the motor driver of the camera lens is generally supplied by a 4.5-5 V voltage output from the boost converter. To ensure fast and accurate focusing of the lens, the peak-to-peak value of the transient overshoot of the motor driver supply voltage must be within 4%-5% of the rated value [1]. For a 28-V DC supply system of military aircraft power systems (as required in MIL-STD-704F [2]), the DC-DC converter output voltage overshoot and undershoot are required to be reduced to 1 V and −6 V within 82.5 ms and 100 ms, respectively, after a change in transient system conditions. It can be seen that, in the practical engineering application, there are clear time-domain dynamic performance index requirements for DC-DC converters.

A variety of dynamic-performance-improvement methods and controls have been proposed for pulse-width modulation (PWM) DC-DC converters. With the cutoff frequency and bandwidth in the frequency domain as the dynamic-performance-improvement objectives, Bode diagram analysis can be used to design dynamic-performance-improvement controls. Several dynamic-performance-improvement controls for PWM DC-DC converters have been proposed using the frequency-domain method to improve the dynamic performance index in the frequency domain; these include three-controller robust average current control [3] and current feedforward average current control [4]. Although these controls can improve the dynamic performance of the PWM DC-DC converter, they are not designed to

Manuscript received January 3, 2023; revised January 31, 2023; accepted February 25, 2023. Date of publication March 31, 2023; date of current version March 5, 2023.

* Corresponding Author, E-mail: hli@bjtu.edu.cn

* Supported by the Key Program of National Natural Science Foundation of China under Grant No. 52237008.

Digital Object Identifier: 10.23919/CJEE.2023.000017

improve the settling time and overshoot index in the time domain, which are the most important factors in practical applications. This makes it difficult for designers to gain a clear understanding of the time-domain dynamic performance index that can be achieved by improved control. Of course, there are also controls based on the time-domain modeling of PWM DC-DC converters that enable the design of time-domain dynamic performance indices, such as settling time or overshoot. With the least linear quadratic function as the control objective [5-6], a linear quadratic regulator (LQR) can be applied to improve the dynamic performance of a PWM DC-DC converter. A linear quadratic function can be composed of different combinations of system state variables. Therefore, different optimal control objectives can be achieved by implementing linear feedback on all the state variables of the system [7]. For example, in Ref. [8], the loss characteristics of a boost converter under a step perturbation were used as a linear quadratic objective function, which enabled the boost converter to have optimal loss characteristics during a dynamic process. Although an LQR can also be designed to improve the time-domain dynamic performance by incorporating settling time and overshoot into the linear quadratic function, it requires full-state feedback, which increases the complexity of the control system. Other control methods based on discrete control, such as deadbeat control [9-10], adjust the duty cycle based on the principle that the controlled variable of the next digital control cycle should be equal to the reference value. Deadbeat control can theoretically achieve a dynamic adjustment of the converter within a limited number of steps in digital control. However, because it ignores the continuous circuit characteristics of the PWM DC-DC converter in each switching mode, the overshoot of the system output cannot be predicted. In fact, when deadbeat control is used, the output of the converter still requires a certain settling time to reach a new steady state during a dynamic process, and the converter still has a certain overshoot [11]. Similar to LQR control, deadbeat control also requires full-state feedback as well as the prediction of the system state variable in the next cycle. Other nonlinear control methods, such as geometric control, can use phase-plane analysis to design the settling time of the PWM DC-DC converter with high precision [12-15]. In Ref. [16], a centric control method that fixed the duty cycle during a dynamic process was proposed. Through a phase-plane analysis, the duty cycle that enables the converter to converge from the initial state to the new steady state can be calculated. The settling time, which can be achieved by centric control, can be precisely designed using the phase-plane method. However, the overshoot of the DC-DC converter cannot be designed. At the same time, as the phase plane can only show the trajectory formed by two state variables, when the system order increases and the number of state variables to be considered increases, the nonlinear geometric control fails.

Although these new controls, based on the time-domain model of the converter, can, to some extent, achieve the design of the time-domain dynamic performance of the PWM DC-DC converter, they cannot improve the time-domain dynamic performance based on the existing stable control of the system. This prevents engineers from quickly improving the control system of the PWM DC-DC converter to meet the specified requirements for settling time and overshoot. Therefore, improving the control of the PWM DC-DC converter based on the existing traditional linear stable control system, such as proportional-integral (PI) or proportional-integral-derivative control, to enhance its dynamic performance would be more attractive to engineers than adopting a completely new control. In this study, a time-domain dynamic-performance-improvement method for PWM DC-DC converters to directly improve the time-domain dynamic performance index is proposed. The proposed dynamic-performance-improvement method can generate a simple improved control that satisfies the required time-domain dynamic performance index based on simple PI or proportional-integral-derivative control.

The remainder of this paper is organized as follows. First, the time-domain dynamic characteristics of the PWM DC-DC converter are quantitatively modeled. In Section 3, the proposed time-domain dynamic-performance-improvement method based on eigenvalues and eigenvector sensitivity (E^2S-based DPIM) is introduced in detail. This section introduces

a method for generating improved controls without the need for additional sampling. In Section 4, using a boost converter with PI control as an example, the proposed dynamic-performance-improvement method is applied to generate an improved control system that can improve the time-domain dynamic performance of the original closed-loop control system. The improved control enables the boost converter to satisfy the specified settling time and overshoot requirements when the output voltage reference undergoes a step change. Finally, the correctness of the proposed time-domain dynamic-performance-improvement method based on power simulation (PSIM) and experiments is verified in Section 5. The time-domain dynamic performance improvement of the boost converter with improved control is also examined. Finally, conclusions are presented in Section 6.

2 Modeling the time-domain dynamic characteristics of the PWM DC-DC converter

Unlike other methods in which completely new controls are designed to achieve time-domain dynamic performance, the proposed dynamic-performance-improvement method directly improves the existing control of the converter to enhance its time-domain dynamic performance. Therefore, considering the impact of the existing control of the converter requires first establishing a time-domain model of the dynamic characteristics of the PWM DC-DC converter under closed-loop control.

2.1 Perturbated dynamic response modeling

A PWM DC-DC converter without any closed-loop control can always be modeled using the following open-loop state-space equation obtained through state-space averaging and small-signal linearization methods

$$\begin{cases} \dot{\boldsymbol{x}} = \boldsymbol{A}_{op}\boldsymbol{x} + \boldsymbol{B}_{op}\boldsymbol{u} + \boldsymbol{E}_{op} \\ \boldsymbol{y} = \boldsymbol{C}_{op}\boldsymbol{x} + \boldsymbol{D}_{op}\boldsymbol{u} \end{cases} \tag{1}$$

where $\boldsymbol{x}$ is an n_0-dimensional state variable vector of the linearized system of the PWM DC-DC converter in open-loop operation; $\boldsymbol{u}$ is the input vector of the system, which is generally the duty cycle signal [17] or phase-shift signal [18] in the PWM DC-DC converter; and $\boldsymbol{y}$ is the output vector of the converter, which is generally the output voltage of the PWM DC-DC converter. $\boldsymbol{A}_{op}$, $\boldsymbol{B}_{op}$, $\boldsymbol{C}_{op}$, $\boldsymbol{D}_{op}$ *and* $\boldsymbol{E}_{op}$ respectively represents the Jacobian matrix, input matrix, output matrix transmission matrix and perturbation matrix of the open loop system. When a continuous controller for closed-loop control is adopted for the PWM DC-DC converter, the closed-loop PWM DC-DC converter system can also be linearized as the following augmented state-space equations

$$\begin{cases} \dot{\boldsymbol{x}}_{cl} = \boldsymbol{A}_{cl}\boldsymbol{x}_{cl} + \boldsymbol{E}_{cl} \\ \boldsymbol{y} = \boldsymbol{C}_{cl}\boldsymbol{x}_{cl} \end{cases} \tag{2}$$

In the closed-loop state-space equation, $\boldsymbol{x}_{cl}$ is an n-dimensional column vector, and the order n-n_0 added to the open-loop state-space equation corresponds to the order of the closed-loop continuous controller. Matrix $\boldsymbol{A}_{cl}$ is the Jacobian matrix of the closed-loop PWM DC-DC converter, and the distribution of its eigenvalues reflects the small-signal stability of the closed-loop control system [19-20]. When the input voltage, load, and reference commands of the PWM DC-DC converter undergo a step change, the output voltage $v_o(t)$ of the PWM DC-DC converter under closed-loop control undergoes a perturbed dynamic process, as shown in Fig. 1.

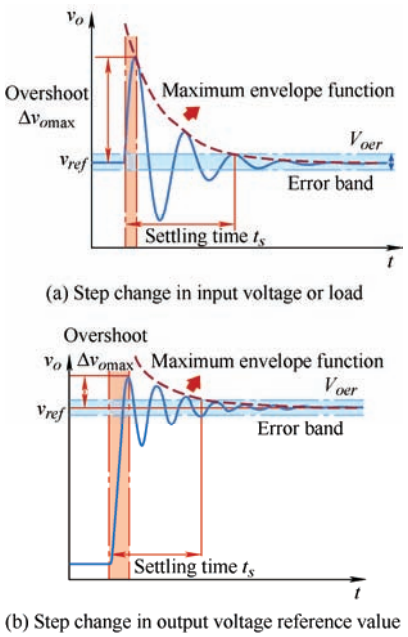

Fig. 1 DC-DC converter dynamic process output voltage

In Fig. 1, the settling time of the closed-loop control system, t_s, is defined as the time from the moment when the disturbance occurs to the time when the output of the system enters the specified error band. The overshoot Δv_{omax} is defined as the maximum output value of the system during the time period from 0 to t_s. In a DC-DC

converter, the size of the error band is generally chosen as half the peak-to-peak value of the output voltage ripple. The dynamic process of the linearized closed-loop PWM DC-DC converter described by Eq. (2) can be transformed into a zero-input response of a linear system. As shown in Fig. 2, the initial value of the zero-input response $\boldsymbol{x}_0$ is the difference between the steady-state values $\boldsymbol{X}_1$ and $\boldsymbol{X}_2$ of the DC-DC converter before and after the disturbance, respectively.

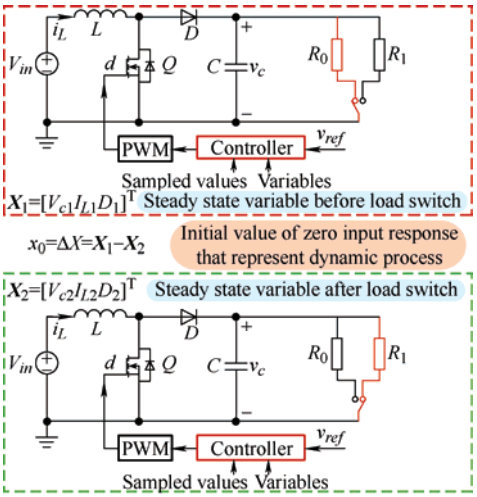

Fig. 2 Equivalence between the DC-DC converter dynamic process during load switching and the zero-input response of a linear system

The zero-input response of a linear system can be succinctly expressed as $\Delta\boldsymbol{x}(t) = \exp(\boldsymbol{A}t)\boldsymbol{x}_0$ using matrix exponential notation [21]. Matrix exponential $\exp(\boldsymbol{A}t)$ can be further diagonalized using the eigenvalue decomposition method. At this point, the zero-input response of the linear system, that is, the dynamic process of the output of the closed-loop control system, can be represented by the eigenvalues and eigenvectors of the closed-loop Jacobian matrix $\boldsymbol{A}_{cl}$, given by [22]

$$\Delta y(t) = \Delta v_o(t) = \sum_{i=1}^{n} \boldsymbol{C}_{cl}\boldsymbol{\varphi}_i\boldsymbol{\psi}_i^{\mathrm{T}}\boldsymbol{x}_0 \exp(\lambda_i t) = \sum_{i=1}^{n} K_i \exp(\lambda_i t) \tag{3}$$

where λ_i is the ith eigenvalue of the closed-loop Jacobian matrix $\boldsymbol{A}_{cl}$, and $\boldsymbol{\varphi}_i$ and $\boldsymbol{\psi}_i^{\mathrm{T}}$ are the right and left eigenvectors corresponding to the ith eigenvalue of $\boldsymbol{A}_{cl}$, respectively. Furthermore, by assuming that the Jacobian matrix of the closed-loop system has m complex eigenvalues and n-m real eigenvalues, the closed-loop control system output represented by Eq. (3) can be transformed into the following damped sinusoidal oscillation using the Euler formula

$$\Delta v_o(t) = \sum_{i=1}^{m} |K_i| \exp(\sigma_i t)\cos(\omega_i t + \theta_i) + \sum_{i=m+1}^{n} K_i \exp(\sigma_i t)$$
$$\theta_i = \arctan\left(\frac{\mathrm{Im}(K_i)}{\mathrm{Re}(K_i)}\right) \tag{4}$$

where σ_i and ω_i are, respectively, the real and imaginary parts of the complex eigenvalue λ_i. According to Eq. (4), each ith sinusoidal damped oscillation formed by an eigenvalue is defined as a subdynamic response, and the corresponding coefficient K_i is defined as the subdynamic coefficient. By using the eigenvalue decomposition method described in Eq. (4), the dynamic process in Fig. 1a can be decomposed into n subdynamic responses, as shown in Fig. 3.

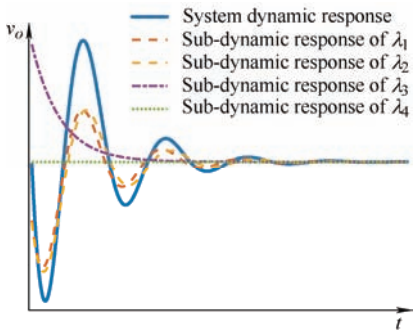

Fig. 3 Decomposition of the PWM DC-DC converter dynamic process output voltage under a load step change according to the eigenvalues

2.2 Settling time and overshoot analysis

The dynamic process of a closed-loop PWM DC-DC converter with a continuous controller can be represented using Eq. (4). Although the expressions in Eq. (4) reflect all the information on the dynamic process of the DC-DC converter, information on the settling time and overshoot is implicit in the equation. Therefore, it is necessary to further search for variables that can directly reflect the settling time and overshoot of closed-loop control systems.

(1) Settling time analysis. For the settling time, as shown in Fig. 1, the time required for the system output to enter the error band is the same as the time required for the red exponential decay envelope line to enter the error band. Therefore, the settling time can be calculated using the envelope functions

$$\Delta v_{oe}(t_s) = \sum_{i=1}^{m} |K_i| \exp(\sigma_i t_s) + \sum_{i=m+1}^{n} K_i \exp(\sigma_i t_s) = V_{oer} \tag{5}$$

In Eq. (5), the settling time t_s is related only to the real part of all eigenvalues of the Jacobian matrix $\boldsymbol{A}_{cl}$

and the subdynamic coefficients K_i. If the distance of all eigenvalues in the left half-plane from the imaginary axis increases and the moduli of all subdynamic coefficients $|K_i|$ decrease, the settling time of the closed-loop control system must decrease. When the error band limit V_{oer} is small, the influence of the modules of the real part of the eigenvalues on the settling time is dominant. In this case, the settling time decreases by the same multiple as the increase in the modulus of the real part of the eigenvalue.

(2) Overshoot analysis. For complex higher order closed-loop control systems, the output voltage overshoot cannot be obtained directly by combining Eq. (4) with an analytical method. However, the overall dynamic response of the closed-loop system represented by Eq. (4) is a linear superposition of the first- or second-order subdynamic responses formed by n eigenvalues, as shown in Fig. 3. Therefore, the overshoot of the system as a whole can be approximated by analyzing the maximum value of each subdynamic response.

For the first-order subdynamic response formed by the real eigenvalues, the maximum value is the modulus of the subdynamic coefficient K_i. The second-order subdynamic responses formed by the complex eigenvalues can be divided into underdamped and overdamped states [23]. In the overdamped state, the maximum value of the response is also the modulus of the subdynamic coefficient. In the underdamped state, the maximum value of its response is referred to as the peak response y_{OS}, which is given as

$$\begin{cases} y_{OSi} = |K_i| N_1 N_2 \qquad \gamma = \dfrac{\sigma_i}{\omega_i} \\ N_1 = \exp\left(\gamma\left[\tan^{-1}(\gamma) - \theta_i + \bar{k}\pi\right]\right) \\ N_2 = \cos\left(\arctan(\gamma) + \bar{k}\pi\right) \end{cases} \tag{6}$$

The correction factor $\bar{k}$ is limited by the time $t_{OSi} > 0$ and is selected to let the second-order subdynamics reach the peak response. $\bar{k}$ is taken to increase gradually from 0. When the peak time $t_{OSi} > 0$, $\bar{k}$ is substituted into Eq. (6), and the value of y_{OSi} when the calculated y_{OSi} is >0 for the first time is the subdynamic peak response. The corresponding constraint is

$$t_{OSi} = \frac{\arctan(\gamma) - \theta_i + \bar{k}\pi}{\omega_i} > 0 \qquad \bar{k} \in N \tag{7}$$

The overshoot of the closed-loop control system must be reduced when the maximum values of all the subdynamic responses are reduced. Furthermore, if a subdynamic response with a dominant role can be determined, it can be assumed that the maximum value of the dominant subdynamic response is the same as that of the entire closed-loop control system.

3 Time-domain dynamic-performance improvement method based on eigenvalue and eigenvector sensitivity

A flowchart of the method for improving the time-domain dynamic performance of PWM DC-DC converters based on eigenvalue and eigenvector sensitivity is shown in Fig. 4. The corresponding principles for improving the dynamic performance of PWM DC-DC converters based on the flowchart in Fig. 4, combined with the definitions of various sensitivities, are introduced in Sections 3.1 and 3.2.

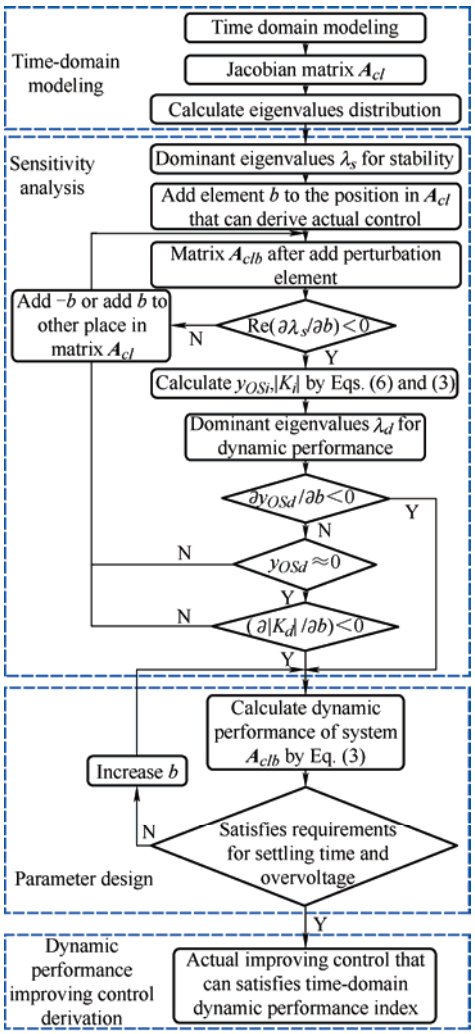

Fig. 4 Flowchart of the time-domain dynamic-performance-improvement method for PWM DC-DC converters based on eigenvalue and eigenvector sensitivity (E^2S-based DPIM)

3.1 Eigenvalue and eigenvector sensitivity

(1) Eigenvalue sensitivity. For a given linear system, the first-order eigenvalue sensitivity of the *i*th eigenvalue λ_i of its Jacobian matrix $\boldsymbol{A}_{cl}$ to a certain parameter *b* in the matrix can be expressed as

$$\frac{\partial \lambda_i}{\partial b}=\frac{\boldsymbol{\psi}_i^{\mathrm{T}}\dfrac{\partial \boldsymbol{A}_{cl}}{\partial b}\boldsymbol{\varphi}_i}{\boldsymbol{\psi}_i^{\mathrm{T}}\boldsymbol{\varphi}_i}\quad\begin{cases}\boldsymbol{A}_{cl}^{\mathrm{T}}\cdot\boldsymbol{\psi}_i=\lambda_i\boldsymbol{\psi}_i\\ \boldsymbol{A}_{cl}\cdot\boldsymbol{\varphi}_i=\lambda_i\boldsymbol{\varphi}_i\end{cases}\tag{8}$$

where $\boldsymbol{\psi}_i^{\mathrm{T}}$ and $\boldsymbol{\varphi}_i$ are, respectively, the left and right eigenvectors of the *i*th eigenvalue. Several eigenvalues of the closed-loop Jacobian matrix $\boldsymbol{A}_{cl}$ closest to the imaginary axis are defined as the dominant eigenvalues λ_s that affect the stability of the closed-loop control system. If the real part of the sensitivity of the dominant eigenvalues λ_s to an additional parameter *b* in the matrix is smaller than 0, this indicates that, after adding parameter *b*, the dominant eigenvalues affecting stability will move away from the imaginary axis. Subsequently, the settling time of the closed-loop control system is shortened, and stability is enhanced.

(2) Eigenvector sensitivity. The first-order eigenvalue sensitivity of the right eigenvector belonging to the *i*th eigenvalue of the closed-loop Jacobian matrix $\boldsymbol{A}_{cl}$ to the parameter *b* in the matrix [24] is defined as

$$\left(\boldsymbol{A}_{cl}-\lambda_i\boldsymbol{E}\right)\frac{\partial \boldsymbol{\varphi}_i}{\partial b}=\left(\frac{\partial \lambda_i\boldsymbol{E}}{\partial b}-\frac{\partial \boldsymbol{A}_{cl}}{\partial b}\right)\boldsymbol{\varphi}_i\tag{9}$$

Because Eq. (9) is a complex equation, to facilitate the calculation, the following method introduced in Ref. [25] was used for the right eigenvector calculation

$$\begin{bmatrix}\boldsymbol{A}_{cl}-\mathrm{Re}(\lambda_i)\boldsymbol{E} & \mathrm{Im}(\lambda_i)\boldsymbol{E}\\ -\mathrm{Im}(\lambda_i)\boldsymbol{E} & \boldsymbol{A}_{cl}-\mathrm{Re}(\lambda_i)\boldsymbol{E}\\ \mathrm{Re}(\boldsymbol{\varphi}_i)^{\mathrm{T}} & \mathrm{Im}(\boldsymbol{\varphi}_i)^{\mathrm{T}}\end{bmatrix}\begin{bmatrix}\mathrm{Re}\left(\dfrac{\partial \boldsymbol{\varphi}_i}{\partial b}\right)\\ \mathrm{Im}\left(\dfrac{\partial \boldsymbol{\varphi}_i}{\partial b}\right)\end{bmatrix}=\begin{bmatrix}\mathrm{Re}\left(\left(\dfrac{\partial \lambda_n}{\partial b}\boldsymbol{E}-\dfrac{\partial \boldsymbol{A}_{cl}}{\partial b}\right)\right)\boldsymbol{\varphi}_i\\ \mathrm{Im}\left(\left(\dfrac{\partial \lambda_n}{\partial b}\boldsymbol{E}-\dfrac{\partial \boldsymbol{A}_{cl}}{\partial b}\right)\right)\boldsymbol{\varphi}_i\\ 0\end{bmatrix}\tag{10}$$

For the left eigenvector, the left eigenvector sensitivity $\partial\boldsymbol{\psi}_i^{\mathrm{T}}/\partial b$ can be calculated by simply replacing all the closed-loop Jacobian matrices $\boldsymbol{A}_{cl}$ in Eq. (10) with their transpose $\boldsymbol{A}_{cl}^{\mathrm{T}}$ and replacing the right eigenvector with the transpose $\boldsymbol{\psi}_i$ of the left eigenvector.

3.2 Subdynamic coefficient sensitivity and subdynamic peak response sensitivity

To analyze the effect of the additional element *b* in the closed-loop Jacobi matrix on the time-domain dynamic performance of the closed-loop control system, the sensitivity of the subdynamic coefficients and the sensitivity of the peak response are defined.

Definition 1: Subdynamic peak response sensitivity $\partial y_{OSi}/\partial b$. The derivative of the damped sinusoidal oscillation peak response y_{OSi} to the added perturbation element *b* in the Jacobian matrix $\boldsymbol{A}_{cl}$ is defined as the subdynamic peak response sensitivity and can be expressed as

$$\frac{\partial y_{OSi}(t)}{\partial b}=\frac{\partial |K_i|}{\partial b}N_1N_2+|K_i|\frac{\partial N_1}{\partial b}N_2+|K_i|N_1\frac{\partial N_2}{\partial b}\tag{11}$$

where $\gamma=\sigma_i/\omega_i$, $\dfrac{\partial N_2}{\partial b}=-\sin\left(\tan^{-1}\gamma\right)\dfrac{\partial \gamma}{\partial b}\dfrac{1}{1+\gamma^2}$, and

$$\frac{\partial N_1}{\partial b}=N_1\left[\frac{\partial \gamma}{\partial b}\left[\tan^{-1}\gamma-\theta_i+\bar{k}\pi\right]+\gamma\left(\frac{\partial \gamma}{\partial b}\frac{1}{\left(1+\gamma^2\right)}-\frac{\partial \theta_i}{\partial b}\right)\right].$$

When the subdynamic peak response sensitivity of complex eigenvalues $y_{OSi}/\partial b$ is smaller than 0, the extra element *b* in the matrix is beneficial in reducing the peak response of the second-order subdynamic formed by this complex eigenvalue.

The further specific derivate expressions are listed in the Appendix.

Definition 2: Subdynamic coefficient sensitivity $\partial K_i/\partial b$. The derivative of coefficients K_i to *b* is defined as the sensitivity of the subdynamic coefficients.

Definition 3: Subdynamic coefficient module sensitivity $\partial|K_i|/\partial b$. The derivative of the module of K_i to *b* is defined as the subdynamic coefficient of the module sensitivity. When the subdynamic coefficient module sensitivity $\partial|K_i|/\partial b$ of real eigenvalues is smaller than 0, the extra element *b* in the matrix is beneficial in reducing the maximum value of the subdynamic response formed by this real eigenvalue.

Subdynamic coefficient sensitivity and subdynamic module sensitivity can be further expressed by left and right eigenvector sensitivity $\partial\boldsymbol{\psi}_i^{\mathrm{T}}/\partial b$ and $\partial\boldsymbol{\varphi}_i/\partial b$, respectively, of the *i*th eigenvalue to *b*. Therefore, the subdynamic peak response sensitivity in Eq. (11) can

be finally expressed by eigenvalue and eigenvector sensitivity. The relationship between the subdynamic coefficient module sensitivity and the eigenvalue and eigenvector sensitivities is shown in the Appendix. Among all the eigenvalues of the closed-loop Jacobian matrix, the eigenvalue with a larger modulus of subdynamic coefficient or subdynamic peak response is defined as the dominant eigenvalue λ_d that affects the dynamic performance of the closed-loop control system. If the subdynamic coefficient or subdynamic peak response of the dominant eigenvalue λ_d decreases, the overshoot of the closed-loop control system will decrease.

3.3 Generation of dynamic-performance-improvement control without additional sampling

According to the flowchart in Fig. 4, if adding element b at a specific location in the matrix can improve the dynamic performance of the closed-loop control system by sensitivity analysis is confirmed, then further improved control can be generated. To avoid additional sampling, a control equivalent to adding element b at a specific location in the Jacobian matrix can be generated by increasing the order of the closed-loop Jacobian matrix $\boldsymbol{A}_{cl}$. A flowchart of the improved control generation method is shown in Fig. 5.

Suppose that the closed-loop Jacobian matrix $\boldsymbol{A}_{clb}$ after adding the extra element b is given by

$$\boldsymbol{A}_{clb}=\begin{bmatrix} a_{cl11} & \cdots & a_{cl1n} \\ \cdots & \cdots+b & \cdots \\ a_{cln1} & \cdots & a_{clnn} \end{bmatrix} \tag{12}$$

where the number of columns with the extra element b is q.

Furthermore, q rows and q columns are added to the original closed-loop Jacobian matrix $\boldsymbol{A}_{cl}$ as

$$\boldsymbol{A}_{ccl}=\begin{bmatrix} \boldsymbol{A}_{cl(n\times n)} & \boldsymbol{X}_{n\times q} \\ \boldsymbol{U}_{q\times n} & \boldsymbol{G}_{q\times q} \end{bmatrix} \tag{13}$$

It should be noted that, in the three added submatrices, the columns of submatrix $\boldsymbol{X}$ are the same as those containing the extra element b in $\boldsymbol{A}_{clb}$. The equivalence matrix $\tilde{\boldsymbol{A}}_{ccl}$ of the augmented closed-loop Jacobian matrix can be obtained using a similar transformation as

$$\boldsymbol{A}_{ccl}\sim\tilde{\boldsymbol{A}}_{ccl}=\begin{bmatrix} \boldsymbol{A}_{clb(n\times n)} & \boldsymbol{X}_{n\times q} \\ \tilde{\boldsymbol{U}}_{n\times q} & \tilde{\boldsymbol{G}}_{n\times q} \end{bmatrix} \tag{14}$$

$\tilde{\boldsymbol{A}}_{ccl}$ contains the matrix $\boldsymbol{A}_{clb}$ after adding element b to the original system Jacobian matrix, which illustrates that the augmented matrix $\boldsymbol{A}_{ccl}$ can achieve similar improvements in the time-domain dynamic performance by adding an element b directly to the closed-loop Jacobian matrix $\boldsymbol{A}_{cl}$.

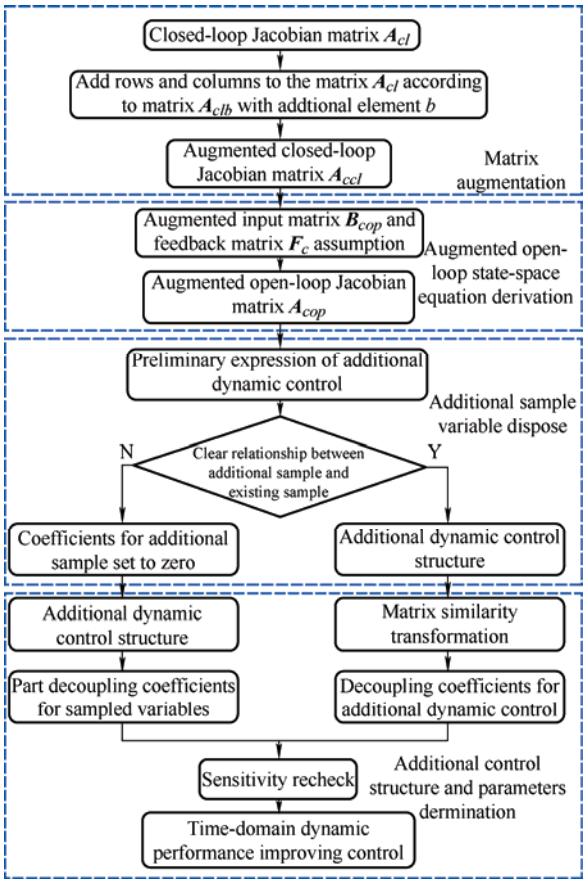

Fig. 5 Flowchart of an improved control generation method equivalent to adding element b to the Jacobian matrix without new sampling

From Fig. 5, by obtaining the open-loop state-space equations corresponding to the augmented closed-loop Jacobian matrix $\boldsymbol{A}_{ccl}$, a preliminary expression for additional dynamic control can be obtained. To avoid adding new samples, the state variables or outputs that have already been sampled are considered to represent the required new state variables. However, if there is no clear relationship between the already sampled variables and unsampled state variables that must be added, only the unsampled state variables can be omitted. Because the necessary new sampling is directly omitted, the impact of the additional element b on the dynamic performance of the closed-loop control system must be reconfirmed through a sensitivity analysis. After processing the newly added sampling,

the parameters of the additional dynamic control can be adjusted to make the $\tilde{\boldsymbol{U}}$ matrix in $\tilde{\boldsymbol{A}}_{ccl}$ a zero matrix, thereby achieving the same dynamic improvement effect as directly adding element b to the original closed-loop Jacobian matrix $\boldsymbol{A}_{cl}$.

4 Example to improve the time-domain dynamic performance of a boost converter with PI control using the proposed method

4.1 Time-domain modeling

A system block diagram of the boost converter with PI control, considering the equivalent series resistance (ESR) of the inductor and capacitor, is shown in Fig. 6.

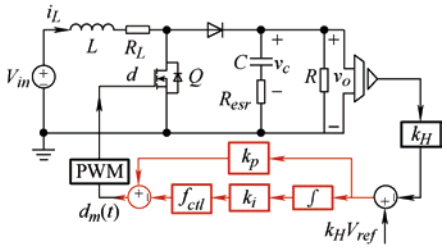

Fig. 6 PI-controlled boost converter with parasitic parameters

The small-signal linearized state-space equations of this closed-loop control system are consistent with Eq. (2), where the state variable $\boldsymbol{x}_{cl}$, the output variable $\boldsymbol{y}$, and the respective matrices are

$$\boldsymbol{x}_{cl}=\left[v_c(t)\ i_L(t)\ d_m(t)\right]^{\mathrm{T}}\quad y=v_o(t) \tag{15}$$

$$\begin{cases}\boldsymbol{A}_{cl}=\begin{bmatrix}\dfrac{-1}{(R+R_{esr})C} & \dfrac{R(1-D)}{(R+R_{esr})C} & -\dfrac{I_L R}{(R+R_{esr})C}\\ \dfrac{(D-1)R}{L(R+R_{esr})} & -\dfrac{RR_{esr}(D-1)^2}{L(R+R_{esr})}+\dfrac{R_L}{L} & \dfrac{V_c}{L}-\dfrac{I_L RR_{esr}(D-1)}{L(R+R_{esr})}\\ a_{cl31} & a_{cl32} & a_{cl33}\end{bmatrix}\\ \boldsymbol{E}_{cl}=\begin{bmatrix}0 & \dfrac{V_{in}}{L} & f_{ctl}k_ik_HV_{ref}\end{bmatrix}^{\mathrm{T}}\\ \boldsymbol{C}_{cl}=\begin{bmatrix}\dfrac{R}{(R+R_{esr})} & \dfrac{RR_{esr}(1-D)}{(R+R_{esr})} & -\dfrac{I_L R_{esr}R}{(R+R_{esr})}\end{bmatrix}\end{cases} \tag{16}$$

where $a_{cl31}=\dfrac{k_pk_H+f_{ctl}k_ik_HR_{esr}C}{(R+R_{esr})C}-f_{ctl}k_ik_H$

$$a_{cl32}=-\frac{(k_pk_H+f_{ctl}k_ik_HR_{esr}C)R(1-D)}{(R+R_{esr})C}$$

$$a_{cl33}=\frac{(k_pk_H+f_{ctl}k_ik_HR_{esr}C)I_LR}{(R+R_{esr})C}$$

The parameters of the main circuit and controller used for the boost converter with PI control in Fig. 6 are listed in Tab. 1. The ESR of the filter inductor and output capacitor were obtained from the datasheets of the corresponding inductor and capacitor, respectively.

Tab. 1 Main circuit and control parameters

Parameter	Value
Input voltage V_{in}/V	18
Output voltage reference V_{ref}/V	24-27
Inductor L/μH	22
Output capacitor C/mF	4.08
Inductor ESR R_L/mΩ	3
Capacitor ESR R_{esr}/mΩ	70
Load resistor R/Ω	8
Sample coefficients k_H	$60.235/2^{23}$
Digital control frequency f_{ctl}/kHz	200
Proportion parameter k_p	100
Integrator parameter k_i	40
Expected settling time t_s/ms	<5
Expected overshoot Δv_o/V	<1

The distribution of the eigenvalues under this control parameter can be calculated, as listed in Tab. 2. Tab. 2 indicates that, because the complex eigenvalues λ_1 and λ_2 are a factor of 100 closer than the real eigenvalues λ_3 from the imaginary axis, the dominant eigenvalues affecting the stability of the boost converter system under PI control are the complex eigenvalues λ_1 and λ_2.

Tab. 2 Eigenvalue distribution for the boost converter with PI control at V_{ref} = 27 V

$\lambda_{1,2}$	λ_3
−64.44 ± j2 836.4	−1 416.3

The open-loop state-space equations of the boost converter with PI control are

$$\begin{cases}\boldsymbol{A}_{op}=\begin{bmatrix}\dfrac{-1}{(R+R_{esr})C} & \dfrac{R(1-D)}{(R+R_{esr})C} & 0\\ \dfrac{(D-1)R}{L(R+R_{esr})} & -\dfrac{RR_{esr}(D-1)^2}{L(R+R_{esr})}-\dfrac{R_L}{L} & 0\\ a_{cl31} & a_{cl32} & 0\end{bmatrix}\\ \boldsymbol{B}_{op}=\begin{bmatrix}-\dfrac{I_LR}{(R+R_{esr})C}\\ \dfrac{V_c}{L}-\dfrac{I_LRR_{esr}(D-1)}{L(R+R_{esr})}\\ \dfrac{(k_pk_H+f_{ctl}k_ik_HR_{esr}C)I_LR}{(R+R_{esr})C}\end{bmatrix}\\ u=d(t)\end{cases} \tag{17}$$

4.2 Sensitivity analysis

Because of the absence of zero elements in the closed-loop Jacobian matrix $\boldsymbol{A}_{cl}$, it is only possible to derive an actual improved control without affecting the characteristics of the main circuit when an entire row or column of the matrix contains additional elements b. Therefore, we considered adding additional elements b to the second column of the closed-loop Jacobian matrix. The closed-loop Jacobian matrix $\boldsymbol{A}_{clb}$ with added element b is

$$\boldsymbol{A}_{clb}=\begin{bmatrix} \dfrac{-1}{(R+R_{esr})C} & \dfrac{R(1-D)}{(R+R_{esr})C}-ba_{cl13} & a_{cl13} \\ \dfrac{(D-1)R}{L(R+R_{esr})} & -\dfrac{RR_{esr}(D-1)^2}{L(R+R_{esr})}+\dfrac{R_L}{L}-ba_{cl23} & a_{cl23} \\ a_{cl31} & a_{cl32}-ba_{cl33} & a_{cl33} \end{bmatrix} \tag{18}$$

where elements a_{cl13} and a_{cl23} are, respectively, the elements of the third column of the first row and the third column of the second row of the original closed-loop Jacobian matrix $\boldsymbol{A}_{cl}$ as given in Eq. (16). The eigenvalue sensitivity of each eigenvalue of $\boldsymbol{A}_{cl}$ to the additional element b was calculated, and results are given in Tab. 3.

Tab. 3 Eigenvalue sensitivity to additional element b = 0.001

$\partial\lambda_{1,2}/\partial b$	$\partial\lambda_3/\partial b$
−498.55±j252.59	−240.81

The sensitivities of all eigenvalues in Tab. 3 is <0, indicating that all the eigenvalues of the closed-loop control system shift away from the imaginary axis when an additional element b is added. The stability of a boost converter with PI control can be enhanced, while the settling time can be reduced. Furthermore, the peak response y_{OS} and the coefficients of each subdynamic were calculated using Eq. (6) and Eq. (3), as presented in Tab. 4.

Tab. 4 Subdynamic peak response and subdynamic coefficients

$y_{OS1,2}$	y_{OS3}	$K_{1,2}$	K_3
0.8	0	0.87	1.58

Tab. 4 shows that, although the subdynamic formed by λ_3 does not constitute damped oscillations, the subdynamic coefficients are large. Therefore, all eigenvalues are dominant eigenvalues that affect the time-domain dynamic performance of the closed-loop control system. The sensitivities of the subdynamic peak response and subdynamic coefficient module were analyzed. The corresponding calculation results are listed in Tab. 5.

Tab. 5 Subdynamic peak response sensitivity and subdynamic coefficient module sensitivity

$\partial y_{OS1,2}/\partial b$	$\partial y_{OS3}/\partial b$	$\partial\lvert K_{1,2}\rvert/\partial b$	$\partial\lvert K_3\rvert/\partial b$
−0.39	0	0.16	−0.09

In Tab. 5, the subdynamic peak response sensitivities of complex eigenvalues λ_1 and λ_2 are <0. Moreover, the subdynamic coefficient module sensitivity of real eigenvalue λ_3 is also <0. This indicates that adding element b is beneficial in reducing the overshoot of the boost converter with PI control. Combining this with the sensitivity analysis results for the eigenvalues listed in Tab. 3, it can be determined that adding element b to the position in $\boldsymbol{A}_{clb}$ as given in Eq. (18) is beneficial for improving the overall time-domain dynamic performance of the closed-loop control system. To set the value of the additional element b, the settling time and overshoot of the closed-loop control system, represented by the Jacobian matrix $\boldsymbol{A}_{cl}$ before and after the addition of element b, were calculated separately. The error band V_{oeb} was set to ±200 mV during the calculation, and the corresponding results are listed in Tab. 6.

Tab. 6 Calculated settling time and overshoot before and after b = 0.001 added to the closed-loop Jacobian matrix $\boldsymbol{A}_{cl}$

Added element	Dynamic performance	
	Settling time	Overshoot
b = 0	33 ms > 5 ms	1.38 V > 1 V
b = 0.001	4.7 ms < 5 ms	0.9 V < 1 V

According to Tab. 6, when the additional element b is 0.001, the closed-loop control system represented by the Jacobian matrix $\boldsymbol{A}_{clb}$ can achieve time-domain dynamic performance requirements of t_s < 5 ms and Δv_o < 1 V for overshoot.

4.3 Additional virtual inductor current feedback control generated by matrix augmentation

In this section, the additional dynamic control generation method introduced in Section 3.3 is used to generate the practical improved control equivalent to the system represented by $\boldsymbol{A}_{clb}$. First, rows and columns were added to the original closed-loop Jacobian matrix $\boldsymbol{A}_{cl}$ to obtain the augmented Jacobian

matrix $\boldsymbol{A}_{ccl}$, and the newly added state variable was set to z. According to Section 3.3, the block matrix form of the augmented Jacobian matrix $\boldsymbol{A}_{ccl}$ is consistent with Eq. (13), where the newly added submatrices $\boldsymbol{X}$, $\boldsymbol{U}$, and $\boldsymbol{G}$ are expressed, respectively, as

$$\boldsymbol{X}=\begin{bmatrix} \dfrac{bI_L R}{(R+R_{esr})C} \\ -\dfrac{bV_c}{L}+\dfrac{bI_L R R_{esr}(D-1)}{L(R+R_{esr})} \\ -\dfrac{b\left(k_p k_H+f_{ctl}k_i k_H R_{esr}C\right)I_L R}{(R+R_{esr})C} \end{bmatrix} \tag{19}$$

$$\boldsymbol{U}=\begin{bmatrix}\alpha_1 & \alpha_2 & \alpha_3\end{bmatrix} \qquad \boldsymbol{G}=g_1 \tag{20}$$

where α_1, α_2, α_3, and g_1 are the elements to be determined in the $\boldsymbol{U}$ and $\boldsymbol{G}$ matrices. The added state variable z is fed back into the duty cycle signal $d(t)$. The feedback matrix $\boldsymbol{F}_c$ of the augmented system based on the small-signal linearization model of the boost converter is

$$\boldsymbol{F}_c=\begin{bmatrix}0 & 0 & 1 & -b\end{bmatrix} \qquad \boldsymbol{B}_{cop}=\begin{bmatrix}\boldsymbol{B}_{op} \\ \beta\end{bmatrix} \tag{21}$$

In a linear system, the closed-loop Jacobian matrix $\boldsymbol{A}_{ccl}$ after the linear feedback of the state variables can be obtained from the linear feedback matrix $\boldsymbol{F}_c$, open-loop Jacobian matrix $\boldsymbol{A}_{cop}$, and input matrix $\boldsymbol{B}_{cop}$ [26], namely, $\boldsymbol{A}_{ccl}=\boldsymbol{A}_{cop}+\boldsymbol{B}_{cop}\boldsymbol{F}_c$. Accordingly, the open-loop Jacobian matrix $\boldsymbol{A}_{cop}$ of the augmented system after additional dynamic control can be obtained in reverse as

$$\boldsymbol{A}_{cop}=\boldsymbol{A}_{ccl}-\boldsymbol{B}_{cop}\boldsymbol{F}_c=$$
$$\begin{bmatrix} \dfrac{-1}{(R+R_{esr})C} & \dfrac{R(1-D)}{(R+R_{esr})C} & 0 & 0 \\ \dfrac{(D-1)R}{L(R+R_{esr})} & -\dfrac{RR_{esr}(D-1)^2}{L(R+R_{esr})}-\dfrac{R_L}{L} & 0 & 0 \\ a_{cl31} & a_{cl32} & 0 & 0 \\ \alpha_1 & \alpha_2 & \alpha_3-\beta & g_1+b\beta \end{bmatrix} \tag{22}$$

By setting the pending coefficient $\beta=\alpha_3$, the open-loop expression of the additional dynamic control can be obtained from Eq. (22) as

$$\dot{z}(t)=\alpha_1 v_c(t)+\alpha_2 i_L(t)+(g_1+b\alpha_3)z(t)+\alpha_3 d(t) \tag{23}$$

In the additional dynamic control represented by Eq. (23), it is necessary to incorporate the unsampled inductor current information. To avoid additional sampling, the output voltage obtained from sampling must be used to represent the inductor current as

$$i_L(t)=\frac{(R+R_{esr})C}{R(1-D)}\frac{\mathrm{d}v_o(t)}{\mathrm{d}t}+\frac{1}{R(1-D)}v_o(t)+\frac{I_L}{(1-D)}d(t) \tag{24}$$

Substituting Eq. (24) into Eq. (23) yields the following additional control open-loop expression without new sampling

$$\dot{z}(t)-W\dot{v}_o(t)=Hv_o(t)+Md(t)+Nz(t) \tag{25}$$

where $W=-\alpha_1 R_{esr}C+\alpha_2\dfrac{(R+R_{esr})C}{R(1-D)}-\dfrac{\alpha_2}{R(1-D)}R_{esr}C$, $H=\alpha_1+\dfrac{\alpha_2}{R(1-D)}$, and $M=\dfrac{\alpha_2 I_L}{(1-D)}+\alpha_3$, $N=g_1+b\alpha_3$.

To avoid differentiation of the output voltage, the intermediate variable $z_c(t)=z(t)-Wv_o(t)$ is defined, and the final expression for the additional dynamic control can be obtained as

$$\begin{cases} z(t)=z_c(t)+Wv_o(t) \\ \dfrac{\mathrm{d}z_c(t)}{\mathrm{d}t}=(H+NW)v_o(t)+Md(t)+Nz_c(t) \end{cases} \tag{26}$$

The corresponding additional dynamic control diagram is shown in Fig. 7.

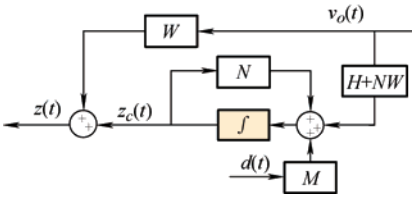

Fig. 7 Additional dynamic control link diagram

Finally, to achieve the same dynamic improvement effect as the additional element b in the original closed-loop Jacobian matrix $\boldsymbol{A}_{cl}$ of the system, the pending parameters α_1, α_2, α_3, and g_1 are set. The matrix $\boldsymbol{A}_{ccl}$ is subjected to a similarity transformation using the transformation matrix

$$\boldsymbol{P}^{-1}=\begin{bmatrix}1 & 0 & 0 & 0 \\ 0 & 1 & 0 & 0 \\ 0 & 0 & 1 & 0 \\ 0 & -1 & 0 & 1\end{bmatrix} \qquad \boldsymbol{P}=\begin{bmatrix}1 & 0 & 0 & 0 \\ 0 & 1 & 0 & 0 \\ 0 & 0 & 1 & 0 \\ 0 & 1 & 0 & 1\end{bmatrix} \tag{27}$$

This results in a similarity matrix $\tilde{\boldsymbol{A}}_{ccl}=\boldsymbol{P}^{-1}\boldsymbol{A}\boldsymbol{P}$ in the same form as Eq. (14). The matrix $\tilde{\boldsymbol{U}}$ is

$$\tilde{\boldsymbol{U}}=\begin{bmatrix}\alpha_1-\dfrac{(D-1)R}{L(R+R_{esr})}\\ \alpha_2+\dfrac{RR_{esr}(D-1)^2}{L(R+R_{esr})}+\dfrac{R_L}{L}+g_1+\dfrac{bV_c}{L}-\dfrac{bI_LRR_{esr}(D-1)}{L(R+R_{esr})}\\ \alpha_3-\dfrac{V_c}{L}+\dfrac{I_LRR_{esr}(D-1)}{L(R+R_{esr})}\end{bmatrix}^{\mathrm{T}} \tag{28}$$

Moreover, because only one row and one column are added to the original closed-loop Jacobian matrix, the matrix $\tilde{\boldsymbol{G}}$ is a scalar.

In Section 3.3, when the submatrix $\tilde{\boldsymbol{U}}$ is a zero matrix, the additional dynamic control shown in Fig. 7 achieves the same effect as the addition of element b to the original closed-loop system Jacobian matrix. At this point, the pending parameters in matrices $\boldsymbol{U}$ and $\boldsymbol{G}$ take the values

$$\begin{cases}\alpha_1=\dfrac{(D-1)R}{L(R+R_{esr})}\\ \alpha_2=-\tilde{G}-\dfrac{RR_{esr}(D-1)^2}{L(R+R_{esr})}-\dfrac{R_L}{L}\\ \alpha_3=\dfrac{V_c}{L}-\dfrac{I_LRR_{esr}(D-1)}{L(R+R_{esr})}\\ g_1=\tilde{G}-\dfrac{bV_c}{L}+\dfrac{bI_LRR_{esr}(D-1)}{L(R+R_{esr})}\end{cases} \tag{29}$$

By setting the scalar $\tilde{G}$, the new eigenvalues introduced by the additional dynamic control shown in Fig. 7 can be controlled. To reduce the impact of this eigenvalue on the dynamic performance of the closed-loop control system, it can be set to a position far enough away from the imaginary axis, such as $\tilde{G}=-3\,000$. Adding the dynamic control loop shown in Fig. 7 to the boost converter with PI control yields the final improved closed-loop control system diagram shown in Fig. 8. Because the inductor current is expressed by the capacitor voltage during control generation, the generated additional dynamic control is called additional virtual inductor current feedback (AVICF) control.

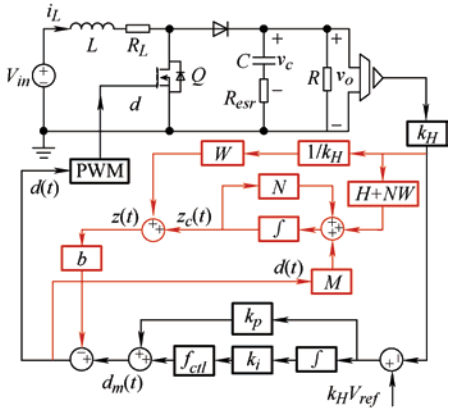

Fig. 8 Additional virtual inductor current feedback control diagram

5 Simulation and experimental verification

5.1 Simulation verification

By using Eq. (4) and Eq. (5), the PI parameter region satisfying the stability and dynamic performance criteria for the original PI-controlled boost converter can be calculated. Furthermore, by utilizing the equivalence of the modified closed-loop Jacobian matrix $\boldsymbol{A}_{clb}$ and AVICF control, the PI parameter region when AVICF control is adopted can be directly calculated using matrices $\boldsymbol{A}_{clb}$ and Eq. (4) and Eq. (5). Moreover, modeling of the AVICF control can be avoided. The corresponding changes in the PI parameter regions are shown in Fig. 9.

Three points were selected to verify the effectiveness of the proposed time-domain dynamic-performance-improvement method. For the boost converter with the PI parameters at point A, the closed-loop control system of the converter cannot operate stably under simple PI control, whereas it can operate stably under AVICF control.

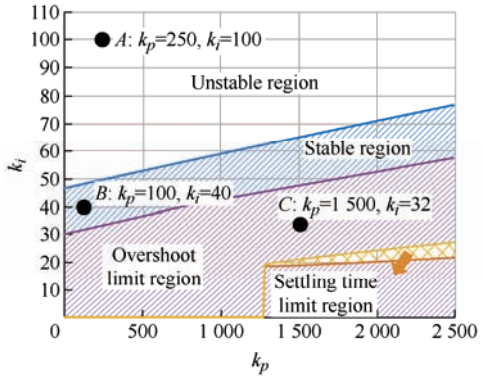

(a) PI parameter region when simple PI control is adopted

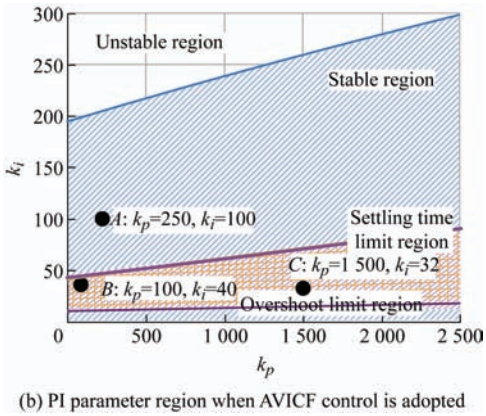

(b) PI parameter region when AVICF control is adopted

Fig. 9 PI parameter region before and after adding AVICF control

For Point *B*, the boost converter with the PI parameters listed in Tab. 1 can operate stably under simple PI control, but the settling time and overshoot cannot satisfy these requirements. When AVICF control is adopted, the closed-loop control system of the boost converter using the PI parameters at point *B* can simultaneously satisfy the settling time and overshoot requirements.

For the boost converter under the PI parameters at point *C*, the overshoot of the closed-loop control system of the converter meets the requirements under simple PI control; however, the settling time cannot meet the requirements. After AVICF control was adopted, the closed-loop control system of the boost converter using the PI parameter can satisfy the given settling time and overshoot requirements. The PSIM simulation waveforms of the output voltage of the boost converter under three types of PI parameters before and after AVICF was adopted are shown in Figs. 10-12.

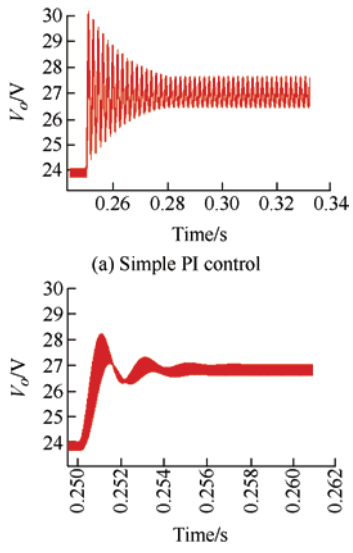

(a) Simple PI control

(b) AVICF control

Fig. 10 Simulation waveform of the boost converter output voltage under the reference step of point *A*

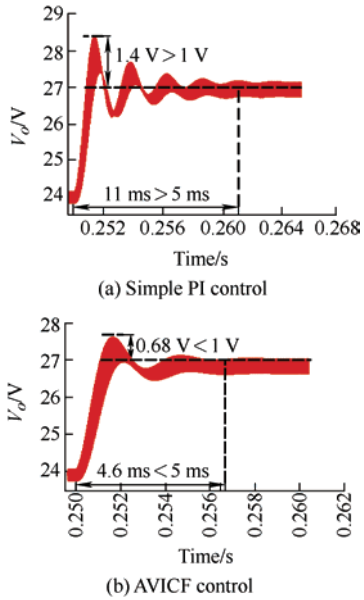

(a) Simple PI control

(b) AVICF control

Fig. 11 Simulation waveform of the boost converter output voltage under the reference step of point *B*

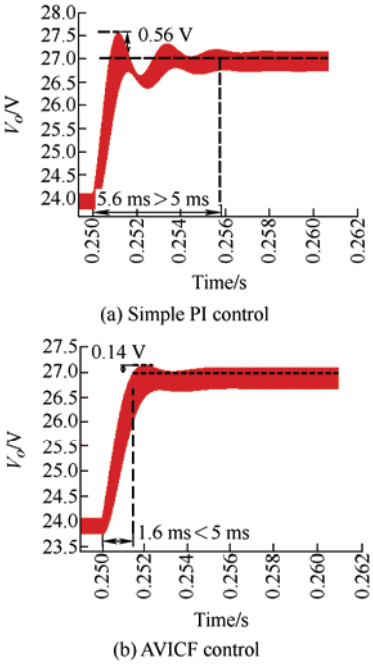

(a) Simple PI control

(b) AVICF control

Fig. 12 Simulation waveform of the boost converter output voltage under the reference step of point *C*

It can be observed from the simulation results in Fig. 10 that, after AVICF control was adopted, the boost converter under the PI parameters at point *A* can operate stably, having been previously unstable after the reference step. The settling time of the boost converter under PI parameters at point *B* was reduced from 11 ms under simple PI control to 4.6 ms, and the overshoot was reduced from 1.4 V to 0.68 V. The overshoot of the converter under PI parameters at point *C* still meets the requirement of being smaller than 1 V after using AVICF control, and the settling

time was reduced from 5.6 ms to 1.6 ms. It can be seen that the boost converter under PI parameters at points *A*, *B*, and *C* can all meet the given requirements of settling time and overshoot in Tab. 1 after AVICF control was adopted.

5.2 Experimental verification

The dynamic performance of the closed-loop control system before and after using AVICF control was verified using an actual boost converter with the same circuit and operating parameters listed in Tab. 1. In the actual boost converter, the main switch (BSC070N10NS5) was used to realize a synchronous boost converter. The main control chip of the circuit (STM32F334) had a maximum frequency of 72 MHz. The circuit used an MTP2920 inductor and a KEM_A4074 capacitor was used for the output capacitance. The corresponding experimental waveforms are shown in Figs. 13-15.

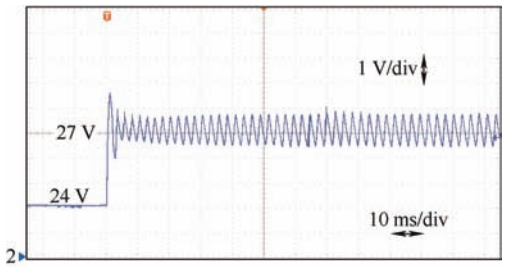

(a) Simple PI control

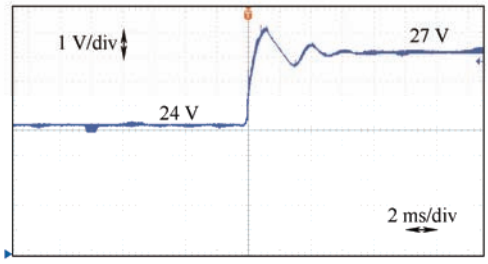

(b) AVICF

Fig. 13 Experimental waveforms of the boost converter output voltage under the reference step of point *A*

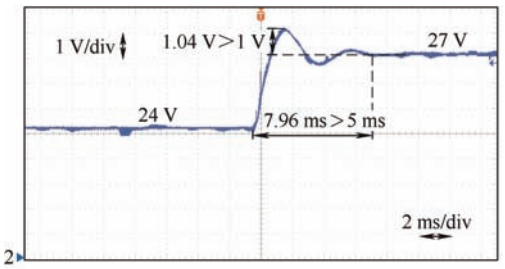

(a) Simple PI control

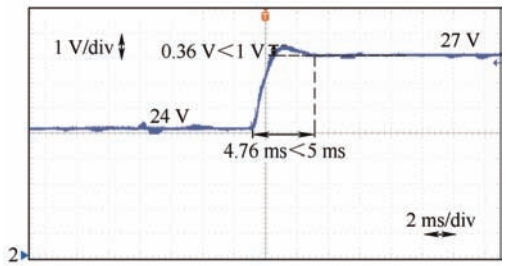

(b) AVICF

Fig. 14 Experimental waveforms of the boost converter output voltage under the reference step of point *B*

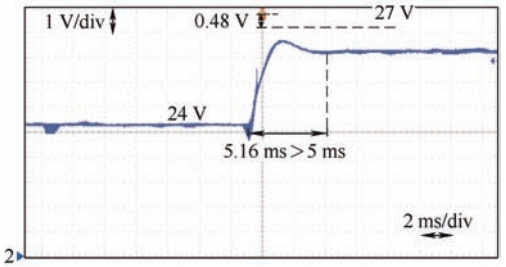

(a) Simple PI control

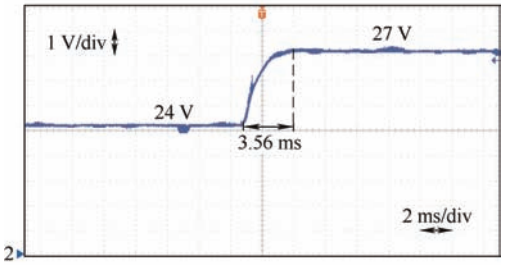

(b) AVICF

Fig. 15 Experimental waveforms of the boost converter output voltage under the reference step of point *C*

The experimental results show that the boost converter under the PI parameters at point *A* stabilizes after AVCIF control was adopted. The boost converter under PI parameters at point *B* does not meet the requirements for overshoot and settling time before AVCIF control was adopted, with an overshoot of 1.09 V and a settling time of 7.96 ms. After using AVCIF control, its overshoot was reduced to 0.36 V, and the settling time was shortened to 4.76 ms, both meeting the requirements. The settling time of the boost converter after AVICF control was adopted was reduced by 40%, and the overshoot was reduced by 65% compared to that of simple PI control. The boost converter under the PI parameters at Point *C* met the requirements for overshoot, but the settling time of 5.16 ms did not meet the requirements under pure PI control. When using AVCIF control, the overshoot was reduced to 0 V, and the settling time was reduced to 3.56 ms, both of which meet the requirements. Owing

to the parasitic parameters in the actual circuit, the potential differences between the values in the datasheet, and the effects of the digital control delay and analog-to-digital converter quantization errors, the experimental waveforms may not be exactly the same as the simulation results. However, the experimental measurements of the settling time and overshoot met the given requirements by adopting AVCIF control. The experimental results demonstrate the effectiveness of the proposed time-domain dynamic-performance-improvement method and the generated AVCIF control.

6 Conclusions

The closed-loop time-domain dynamic performance of PWM DC-DC converters can be accurately represented by the eigenvalues and eigenvectors of the Jacobian matrix obtained by linearizing the converter with state-space averaging. Based on this principle, a time-domain dynamic-performance-improvement method for PWM DC-DC converters based on eigenvalues and eigenvector sensitivity (E^2S-based DPIM) is proposed. The impact of the additional disturbance elements in the Jacobian matrix on the time-domain dynamic performance of the closed-loop control system of PWM DC-DC converters can be quantitatively described by the eigenvalue and eigenvector sensitivities. Furthermore, the improved control which are beneficial to improve the dynamic performance of the closed-loop control system without the need for additional sampling can be generated by extending the closed-loop Jacobian matrix. In a boost converter with PI control, AVICF control that does not require additional sampling can be generated using the proposed dynamic-performance-improvement method. Under a specific set of PI control parameters, the settling time of the boost converter with AVICF control can be reduced by 40%, and the overshoot can be reduced by 65% compared with values obtained using only PI control.

Appendix

Two of the derivative terms in the subdynamic peak response sensitivity are

$$\frac{\partial \gamma}{\partial b}=\frac{\mathrm{Re}\left(\frac{\partial \lambda_i}{\partial b}\right)\omega_i-\mathrm{Im}\left(\frac{\partial \lambda_i}{\partial b}\right)\sigma_i}{\omega_i^2} \tag{A1}$$

$$\frac{\partial \theta_i}{\partial b}=\frac{\mathrm{Im}\left(\frac{\partial K_i}{\partial b}\right)\mathrm{Re}\left(K_i\right)-\mathrm{Re}\left(\frac{\partial K_i}{\partial b}\right)\mathrm{Im}\left(K_i\right)}{\left(1+\left(\frac{\mathrm{Im}\left(K_i\right)}{\mathrm{Re}\left(K_i\right)}\right)^2\right)\mathrm{Re}^2\left(K_i\right)} \tag{A2}$$

The subdynamic coefficient module sensitivity was calculated from the eigenvalue and eigenvector sensitivity using the following formulas

$$\frac{\partial |K_i|}{\partial b}=\frac{\xi}{2|K_i|\left(\mathrm{Re}\left(\boldsymbol{\psi}_i^{\mathrm{T}}\boldsymbol{\varphi}_i\right)^2+\mathrm{Im}\left(\boldsymbol{\psi}_i^{\mathrm{T}}\boldsymbol{\varphi}_i\right)^2\right)^2} \tag{A3}$$

$$\begin{cases}\dfrac{\partial\left(\boldsymbol{C}_{cl}\boldsymbol{\varphi}_i\right)}{\partial b}=\boldsymbol{C}_{cl}\dfrac{\partial\boldsymbol{\varphi}_i}{\partial b}\\ \dfrac{\partial\left(\boldsymbol{\psi}_i^{\mathrm{T}}\boldsymbol{x}_0\right)}{\partial b}=\dfrac{\partial\boldsymbol{\psi}_i^{\mathrm{T}}}{\partial b}\boldsymbol{x}_0+\boldsymbol{\psi}_i^{\mathrm{T}}\dfrac{\partial\boldsymbol{x}_0}{\partial b}\\ \dfrac{\partial\left(\boldsymbol{\psi}_i^{\mathrm{T}}\boldsymbol{\varphi}_i\right)}{\partial b}=\dfrac{\partial\boldsymbol{\psi}_i^{\mathrm{T}}}{\partial b}\boldsymbol{\varphi}_i+\boldsymbol{\psi}_i^{\mathrm{T}}\dfrac{\partial\boldsymbol{\varphi}_i}{\partial b}\quad \dfrac{\partial\boldsymbol{\psi}_i^{\mathrm{T}}}{\partial b}=\left(\dfrac{\partial\boldsymbol{\psi}_i}{\partial b}\right)^{\mathrm{T}}\end{cases} \tag{A4}$$

$$\begin{aligned}\xi=&\begin{bmatrix}2\left[\mathrm{Re}\left(\boldsymbol{C}_{cl}\boldsymbol{\varphi}_i\right)\mathrm{Re}\left(\boldsymbol{\psi}_i^{\mathrm{T}}\boldsymbol{x}_0\right)-\mathrm{Im}\left(\boldsymbol{C}_{cl}\boldsymbol{\varphi}_i\right)\mathrm{Im}\left(\boldsymbol{\psi}_i^{\mathrm{T}}\boldsymbol{x}_0\right)\right]\left[\begin{matrix}\dfrac{\partial\mathrm{Re}\left(\boldsymbol{C}_{cl}\boldsymbol{\varphi}_i\right)}{\partial b}\mathrm{Re}\left(\boldsymbol{\psi}_i^{\mathrm{T}}\boldsymbol{x}_0\right)+\mathrm{Re}\left(\boldsymbol{C}_{cl}\boldsymbol{\varphi}_i\right)\dfrac{\partial\mathrm{Re}\left(\boldsymbol{\psi}_i^{\mathrm{T}}\boldsymbol{x}_0\right)}{\partial b}-\\ \dfrac{\partial\mathrm{Im}\left(\boldsymbol{C}_{cl}\boldsymbol{\varphi}_i\right)}{\partial b}\mathrm{Im}\left(\boldsymbol{\psi}_i^{\mathrm{T}}\boldsymbol{x}_0\right)-\mathrm{Im}\left(\boldsymbol{C}_{cl}\boldsymbol{\varphi}_i\right)\dfrac{\partial\mathrm{Im}\left(\boldsymbol{\psi}_i^{\mathrm{T}}\boldsymbol{x}_0\right)}{\partial b}\end{matrix}\right]+\\ 2\left[\mathrm{Re}\left(\boldsymbol{C}_{cl}\boldsymbol{\varphi}_i\right)\mathrm{Im}\left(\boldsymbol{\psi}_i^{\mathrm{T}}\boldsymbol{x}_0\right)+\mathrm{Im}\left(\boldsymbol{C}_{cl}\boldsymbol{\varphi}_i\right)\mathrm{Re}\left(\boldsymbol{\psi}_i^{\mathrm{T}}\boldsymbol{x}_0\right)\right]\left[\begin{matrix}\dfrac{\partial\mathrm{Re}\left(\boldsymbol{C}_{cl}\boldsymbol{\varphi}_i\right)}{\partial b}\mathrm{Im}\left(\boldsymbol{\psi}_i^{\mathrm{T}}\boldsymbol{x}_0\right)+\mathrm{Re}\left(\boldsymbol{C}_{cl}\boldsymbol{\varphi}_i\right)\dfrac{\partial\mathrm{Im}\left(\boldsymbol{\psi}_i^{\mathrm{T}}\boldsymbol{x}_0\right)}{\partial b}+\\ \dfrac{\partial\mathrm{Im}\left(\boldsymbol{C}_{cl}\boldsymbol{\varphi}_i\right)}{\partial b}\mathrm{Re}\left(\boldsymbol{\psi}_i^{\mathrm{T}}\boldsymbol{x}_0\right)+\mathrm{Im}\left(\boldsymbol{C}_{cl}\boldsymbol{\varphi}_i\right)\dfrac{\partial\mathrm{Re}\left(\boldsymbol{\psi}_i^{\mathrm{T}}\boldsymbol{x}_0\right)}{\partial b}\end{matrix}\right]\end{bmatrix}\left[\mathrm{Re}\left(\boldsymbol{\psi}_i^{\mathrm{T}}\boldsymbol{\varphi}_i\right)^2+\mathrm{Im}\left(\boldsymbol{\psi}_i^{\mathrm{T}}\boldsymbol{\varphi}_i\right)^2\right]-\\ &\left[2\mathrm{Re}\left(\boldsymbol{\psi}_i^{\mathrm{T}}\boldsymbol{\varphi}_i\right)\frac{\partial\mathrm{Re}\left(\boldsymbol{\psi}_i^{\mathrm{T}}\boldsymbol{\varphi}_i\right)}{\partial b}+2\mathrm{Im}\left(\boldsymbol{\psi}_i^{\mathrm{T}}\boldsymbol{\varphi}_i\right)\frac{\partial\mathrm{Im}\left(\boldsymbol{\psi}_i^{\mathrm{T}}\boldsymbol{\varphi}_i\right)}{\partial b}\right]\begin{bmatrix}\left[\mathrm{Re}\left(\boldsymbol{C}_{cl}\boldsymbol{\varphi}_i\right)\mathrm{Re}\left(\boldsymbol{\psi}_i^{\mathrm{T}}\boldsymbol{x}_0\right)-\mathrm{Im}\left(\boldsymbol{C}_{cl}\boldsymbol{\varphi}_i\right)\mathrm{Im}\left(\boldsymbol{\psi}_i^{\mathrm{T}}\boldsymbol{x}_0\right)\right]^2+\\ \left[\mathrm{Re}\left(\boldsymbol{C}_{cl}\boldsymbol{\varphi}_i\right)\mathrm{Im}\left(\boldsymbol{\psi}_i^{\mathrm{T}}\boldsymbol{x}_0\right)+\mathrm{Im}\left(\boldsymbol{C}_{cl}\boldsymbol{\varphi}_i\right)\mathrm{Re}\left(\boldsymbol{\psi}_i^{\mathrm{T}}\boldsymbol{x}_0\right)\right]^2\end{bmatrix}\end{aligned} \tag{A5}$$

References

[1] Y Luo, C Chiou, C Wu, et al. Transient improvement by window transient enhancement and overshoot suppression techniques in current mode boost converter. *IEEE Transactions on Power Electronics*, 2011, 26(10): 2753-2761.

[2] U.S. Department of defense. MTL-STD-704F-2013 Aircraft electric power characteristics.

[3] G Garcera, E Figueres, A Mocholi. Novel three-controller average current mode control of DC-DC PWM converters with improved robustness and dynamic response. *IEEE Transactions on Power Electronics*, 2000, 15(3): 516-528.

[4] P Chrin, C Bunlaksananusorn. Novel current feedforward average current mode control technique to improve output dynamic performance of DC-DC converters. *2007 7th International Conference on Power Electronics and Drive Systems*, Nov. 27-30, 2007, Bangkok, Thailand. IEEE, 2007: 1416-1421.

[5] R M T R Ismail, M A Ahmad, M S Ramli. Speed control of buck-converter driven dc motor using LQR and PI: A comparative assessment. *2009 16th International Conference on Information Management and Engineering*, Oct. 21-23, 2009, Kuala Lumpur, Malaysia. IEEE, 2009: 651-655.

[6] C Olalla, R Leyva, A El Aroudi, et al. Robust LQR control for PWM converters: An LMI approach. *IEEE Transactions on Industrial Electronics*, 2009, 56(7): 2548-2558.

[7] M Zhang, X Li, J Liu, et al. Dual-mode LQR-feedforward optimal control for non-minimum phase boost converter. *IET Power Electronics*, 2017, 10(1): 92-102.

[8] D O Neacsu, A Sirbu. Design of a LQR-based boost converter controller for energy savings. *IEEE Transactions on Industrial Electronics*, 2019, 67(7): 5379-5388.

[9] A Iskhakov, Y Portnoy, S Skovpen, et al. Direct deadbeat control of a buck converter. *IECON 2019 - 45th Annual Conference of the IEEE Industrial Electronics Society*, Oct. 14-17, 2019, Lisbon, Portugal. IEEE, 2019: 347-352.

[10] S Saeed, W Zhao, H Wang, et al. Fault-tolerant deadbeat model predictive current control for a five-phase PMSM with improved SVPWM. *Chinese Journal of Electrical Engineering*, 2021, 7(3): 111-123.

[11] S Wei, Z Zhao, K Li, et al. Deadbeat current controller for bidirectional dual-active-bridge converter using an enhanced SPS modulation method. *IEEE Transactions on Power Electronics*, 2020, 36(2): 1274-1279.

[12] W W Burns, T G Wilson. A state-trajectory control law for DC-to-DC converters. *IEEE Transactions on Aerospace and Electronic Systems*, 1978, AES-14(1): 2-20.

[13] V Li, Q Li, F C Lee. Improved V^2 constant on-time control with state-trajectory control. *2020 IEEE Applied Power Electronics Conference and Exposition (APEC)*, March 15-19, 2020, New Orleans, LA, USA. IEEE, 2020: 3031-3038.

[14] K Hariharan, S Kapat. Near optimal controller tuning in a current-mode DPWM Boost converter in CCM and application to a dimmable LED array driving. *IEEE Journal of Emerging and Selected Topics in Power Electronics*, 2019, 7(2): 1031-1043.

[15] I G Zurbriggen, F Degioanni, M Ordonez. Near-time-optimal dynamics in PWM DC-DC converters: Dual-loop geometric control. *IEEE Journal of Emerging and Selected Topics in Power Electronics*, 2021, 9(1): 167-182.

[16] I G Zurbriggen, M Ordonez, M Anun. PWM-geometric modeling and centric control of basic DC-DC topologies for sleek and reliable large-signal response. *IEEE Transactions on Industrial Electronics*, 2015, 62(4): 2297-2308.

[17] F E Thau. A feedback compensator design procedure for switching regulators. *IEEE Transactions on Industrial Electronics and Control Instrumentation*, 1979, IECI-26(2): 104-110.

[18] S Zhang, K Li, Y Liang, et al. Generalized state-space averaging modeling of dual-active-bridge converter with triple-phase-shift control. *2022 IEEE International Power Electronics and Application Conference and Exposition (PEAC)*, Nov. 4-7, 2022, Guangzhou, Guangdong, China. IEEE, 2022: 705-710.

[19] H Li, F Ren, C Liu, et al. An extended stability analysis method for paralleled DC-DC converters system with considering the periodic disturbance based on Floquet theory. *IEEE Access*, 2020, 8: 9023-9036.

[20] Z Guo, H Li, C Liu, et al. Stability-improvement method of cascaded DC-DC converters with additional voltage-error mutual feedback control. *Chinese Journal of Electrical Engineering*, 2019, 5(2): 63-71.

[21] C Moler, C Van Loan. Nineteen dubious ways to compute the exponential of a matrix. *SIAM Review*, 2003, 45(1): 3-49.

[22] J P Hespanha. Solutions to LTI systems, linear systems theory. 2nd Ed. Princeton: Princeton University Press, 2018.

[23] J B Cobos. Parameter estimation for an overdamped dynamic second order system, a new approach. *2021 IEEE 5th Colombian Conference on Automatic Control*

(CCAC), Oct. 19-22, 2021, Ibague, Colombia. IEEE, 2021: 43-48.

[24] T B Crossley, B Porter. Eigenvalue and eigenvector sensitivities in linear systems theory. *International Journal of Control*, 1969, 10(2): 163-170.

[25] J E Condren, T W Gedra. Eigenvalue and eigenvector sensitivities applied to power system steady-state operating point. *The 2002 45th Midwest Symposium on Circuits and Systems, 2002. MWSCAS-2002*, Aug. 4-7, 2002, Tulsa, OK, USA. IEEE, 2002: I-683.

[26] J W Choi, J G Lee, Y Kim, et al. Design of an effective controller via disturbance accommodating left eigenstructure assignment. *Journal of Guidance, Control, and Dynamics*, 1995, 18(2): 347-354.

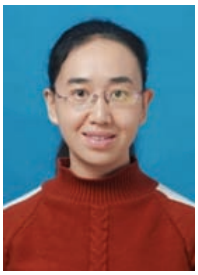

Hong Li received the B.Sc. degree in Electrical Engineering from Taiyuan University of Technology, Taiyuan, China, in 2002, M.Sc. degree in Electrical Engineering from South China University of Technology, Guangzhou, China, in 2005, and Ph.D. degree in Electrical Engineering from Fern Universität in Hagen, Germany, in 2009.

She is currently a Full Professor with the School of Electrical Engineering, Beijing Jiaotong University, Beijing, China. She has published 1 book, 68 journal papers, and 61 conference papers. She has also authorized 30 patents. Her research interests include nonlinear modeling, analysis and its applications, EMI suppressing methods for power electronic systems, and wide bandgap power devices and applications.

Dr. Li is an Associate Editor of the IEEE Transactions on Industrial Electronics, an Associate Editor of the IEEE Open Journal of Industrial Electronics Society, an Associate Editor of the Chinese Journal of Electrical Engineering, and the Vice Chairman of Electromagnetic Compatibility Specialized Committee in China Power Supply Society.

Zexi Zhou was born in Hubei, China, in 1997. He received the B.S. degree in Beijing University of Civil Engineering and Architecture, Beijing, China, in 2020. He is currently working toward the M.S. degree in Electrical Engineering at the School of Electrical Engineering, Beijing Jiaotong University, Beijing, China. His current research interests are stability and dynamic performance analysis of power electronics systems.

Jinchang Pan was born in Hubei, China, in 1999. He received the B.S. degree in Yanshan University, Qinhuangdao, Hebei China, in 2021. He is currently working toward the M.S. degree in Electrical Engineering at the School of Electrical Engineering, Beijing Jiaotong University, Beijing, China. His current research interests are nonlinear modeling and analysis of power electronic systems.

Qian Liu was born in Shanxi, China, in 1998. She received the B.S. degree in Taiyuan University of Technology, Taiyuan, Shanxi, China, in 2020. She is currently working toward the M.S. degree in Electrical Engineering at the School of Electrical Engineering, Beijing Jiaotong University, Beijing, China. Her current research interests are nonlinear modeling and analysis of power electronic systems.